metals

MDPI

Article

The Influence of Laser Welding on the Mechanical Properties of Dual Phase and Trip Steels

Emil Evin [1] and Miroslav Tomáš [2,*]

[1] Department of Automotive Production, Faculty of Mechanical Engineering, Technical University of Košice, Mäsiarska 74, 040 01 Košice, Slovakia; emil.evin@tuke.sk
[2] Department of Computer Support of Technology, Faculty of Mechanical Engineering, Technical University of Košice, Mäsiarska 74, 040 01 Košice, Slovakia
* Correspondence: miroslav.tomas@tuke.sk; Tel.: +421-55-602-3524

Received: 6 June 2017; Accepted: 26 June 2017; Published: 29 June 2017

Abstract: Nowadays, a wide range of materials is used for car body structures in order to improve both the passengers' safety and fuel consumption. These are joined by laser welding and solid state fiber lasers being used more and more in present. The article is focused on the research of laser welding influence on the mechanical and deformation properties, microstructure and microhardness of advanced high-strength steels: high-strength low-alloyed steel HC340LA, dual phase steel HCT600X and multi-phase residual austenite steel RAK40/70. The proper welding parameters have been found based on weld quality evaluation. The specimens for tensile test with longitudinal laser weld were used to measure mechanical and deformation properties. Microstructure and microhardness of laser welds were evaluated in the base metal, heat affected zone and fusion zone. The higher values of strength and lower ones for deformation properties of laser-welded materials have been found for dual and multi-phase steel. The microhardness strongly depends on the carbon equivalent of steel. Deformation properties are more sensitive than strength properties to the change of microstructure in the fusion zone and heat affected zone.

Keywords: laser welds; mechanical properties; low alloyed steel; dual phase steel; trip steel

1. Introduction

In the automotive industry, an emphasis on inventions, innovations and information is reflected in the constant increase of car models in the portfolio of individual automakers. On the one hand, this is due to intensification of individualism with current absolute orientation of enterprises on the customer, and, on the other hand, this is due to the models' diversification of vehicle manufacturers in terms of marketing of various technological innovations and new vehicle concepts on the market, with the aim to occupy the greatest number of market segments. Customers also demand cars that will respect their individual needs, and it affects not only the actual increase in the number of models on offer, but also increases the complexity of the car and a separate system.

Today, it is expected in the automotive industry that, based on the material selection strategies, such products are introduced to the market, involving more intellect and less material. Materials also have a close relationship to the passive safety of vehicles. While the vehicle's car body is the important passive safety component, the lives of the passengers and the other transport users depend on strength and deformation properties of the material. The car body designers have to choose materials with exact properties to control the deformation of each car body structural component. In the frontal deformation zones, materials able to absorb as much impact energy as possible on a larger path should be used. Otherwise, in the middle zone of the car-body, strong materials able to absorb impact energy on a shorter path (minimum deformation) should be used. The innovative potential of the thin-walled lightweight (shell) structures from aluminum alloys, magnesium alloys, composites, High Strength

Steels (HSS) and Ultra High Strength Steels (UHSS) is a big challenge when looking for the right material for each deformation zone [1,2].

Light-weight alloy materials used in the car body structural components are undoubtedly of great potential for lightening many structural parts of the cars. However, the overall share of steel still exceeds 50% of the total weight of the mass-produced cars. The uniqueness of the position of steel in the construction of cars is determined by the combination of its properties such as strength, stiffness, deformation work, formability and recyclability [2,3].

Standard low alloyed high-strength steels (IF, BH, and HSLA), advanced high-strength steels (AHSS) and ultra high-strength steels (UHSS—DP, CP, TRIP, TWIP and MS steels) commonly used in the automotive industry differ in their microstructure. Properties of steels are controlled by chemical composition and the strengthening mechanisms, such as: hardening by solid solutions, dislocation hardening, grain boundaries hardening, precipitation or transformation hardening [4].

The research in the paper is focused on the high strength low alloyed steel, dual phase steel and multiphase steel. In the case of high-strength low-alloy (HSLA) steels, the increase of the ferritic matrix strength is achieved especially by microalloying elements Ti, V, and Nb, which increase strength by grain size control, precipitation hardening, or substitution hardening of structure [4,5]. Dual phase steels consist of a ferritic matrix with 5% to 30% martensite content. Ferrite is a soft phase with good formability. Martensite is a hard phase that gives the material its strength and hardness [4,6]. Transformation induced plasticity (TRIP) steels consist of retained austenite, martensite, bainite and ferrite. Residual austenite transforms to martensite during deformation, and it is situated in the polygonal ferritic matrix, which also includes bainite, preserving very good formability [4,7]. Both dual phase and multi-phase steels show more work hardening (WH) and bake hardening (BH) (Figure 1a,b) than high strength low alloyed steel [3].

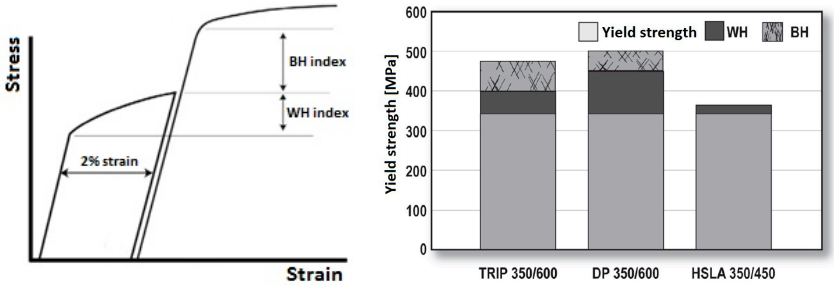

Figure 1. Contribution of work and bake hardening for some advanced high strength steels: (**a**) the effect of both, work hardening (WH) and bake hardening (BH) on the stress–strain curve; (**b**) comparison of the WH and BH for transformation induced plasticity—TRIP, dual phase—DP and high strength low alloyed steel—HSLA steel at a 2% level of strain [3].

Structural thin-walled components of security zones of cars must often meet conflicting requirements—on the one hand, the growing tendency for the reduction of the weight of stamped body parts and, on the other hand, the tendency of increasing the security (strength, stiffness, absorption capacity and programmable deformability under crash). The desired compromise between the requirements to reduce the weight of cars on the one hand and requirements for improving the safety parameters (strength, stiffness, both deformation and fatigue works), reduction of fuel consumption and emissions during operation of cars on the other hand, can be achieved by proper application of the combined tailored blanks: tailor-welded blanks (TWB), engineering blanks (EB), tailor-rolled blanks (TRB), tailor heat treated blanks (THTB) (with the same or different thickness, with different strength and deformation properties, especially in the deformation zones of thin-walled components of cars) [8–11]. The combined TWBs prepared by laser beam or electron beam welding have found the widest application.

In the areas with smaller load, the sheet metal with reduced thickness or less expensive material of less strength is applied. In the areas where greater loads occur, the material of greater thickness and higher strength is applied. Because of these advantages, combined blanks are widespread in the design of car body components and also improve their utility properties (e.g., stainless austenitic and ferritic steels for improving the corrosion resistance in the exhaust systems, the fuel tanks, etc.). According to the data of suppliers of materials for the automotive industry, their share in the structure of the car body should be increased in the coming years up to 30% [12,13].

Application of solid-state lasers in the industry currently comes with a significantly increasing perspective, especially due to the fact that new types of solid-state lasers such as fiber and disk lasers with their technical parameters surpass the parameters of gas CO_2 lasers [14,15].

The most important advantages of solid-state lasers include:

1. Conversion efficiency of electric energy to the energy of the laser beam being higher by 30% compared to the CO_2 lasers,
2. Higher focusability that expands the field of industrial applicability,
3. Improved flexibility and stability of output parameters,
4. Increased dynamics of beam parameters with the possibility of shaping the rise and decay, and the tip of the laser pulse.

Research results of weldability and formability indicate that influence of welded joints on the material plastic flow in the joint area is examined and analyzed by the same kind of tests as are used for evaluation of weldability and formability of base materials, when used for TWBs: tensile tests; braking tests; technological tests (cup drawing tests, Erichsen tests, the Swift method, hydraulic bulge tests, hole expanding test, limit dome height tests and three- or four-point bending tests); macro and microstructure analyses of individual zones of welded joints; hardness tests and Vickers micro-hardness in zones of welded joints and the base material [16,17].

The aim of the paper is to assess the impact of laser welding on the mechanical properties of selected AHSS materials for TWBs, used in the automotive industry for structural components of the car body. The study is focused on the measurement of strength and deformation properties for base material and laser welded by a solid-state fiber laser. Many authors have investigated the influence of laser welding on the tensile properties on specimens with transverse weld [5,6,18–20]. Thus, the research was focused on the specimens with longitudinal butt laser weld, as it is used for tailored TWBs. It is supposed that the longitudinal weld is more sensitive to the stress–strain distribution when a tensile test is performed. In addition, the microstructural changes and microhardness in the heat affected zone and fusion zone were examined.

2. Materials and Methods

The experimental research has been focused on the high strength low alloyed steel HC340LA, dual phase steel HCT600X and multi-phase residual austenite steel RAK40/70. Steels were electrolytically coated with zinc (100 g/m^2) and had special requirements for surface (M—normal surface finish, B—best quality, O—oiled). These are commonly used to enhance the safety characteristics—strength, stiffness, and deformation work—and reduce both the fuel consumption and car emissions. The chemical composition of materials, shown in Table 1, was measured by atomic emission spectrometry according to standard ASTM E415-14.

The first stage of the experimental research was focused on analyzing the influence of laser welding on mechanical and deformation properties of laser-welded base material HC340LA-HC340LA, HCT600X-HCT600X and RAK40/70-RAK40/70 when welded by a solid state fiber laser YLS-5000 (IPG Photonics, Oxford, MA, USA). The welding was done by continual mode without protective gas with parameters shown in Table 2. Samples for microstructure analysis taken from laser-welded sheets have been analyzed by an optical microscope Axio Observer 1M (Carl Zeiss Jena GmbH, Jena, Germay). The welding parameters have been optimized by quality control based on weld porosity

and weld root quality in the heat affected zone and fusion zone. Optimized weld parameters were used to prepare samples for the research.

Table 1. Chemical composition of materials used for research.

Material	Chemical Composition wt %								
HC340LA	C	Si	Mn	P	S	Cu	Al	Cr	Mo
	0.083	0.039	0.181	0.038	<0.002	0.081	0.062	0.044	0.034
	Ni	V	Ti	Nb	Co	W		CE_Y acc. to (1)	
	0.048	0.018	<0.002	0.071	0.155	-		0.122	
HCT600X	C	Si	Mn	P	S	Cu	Al	Cr	Mo
	0.111	0.279	1.963	0.026	<0.002	0.019	0.031	0.206	<0.002
	Ni	V	Ti	Nb	Co	W		CE_Y acc. to (1)	
	<0.002	0.012	<0.002	0.02	0.017	<0.005		0.397	
RAK40/70	C	Si	Mn	P	S	Cu	Al	Cr	Mo
	0.197	0.165	1.576	0.015	<0.002	0.022	1.352	0.0455	0.022
	Ni	V	Ti	Nb	Co	W		CE_Y acc. to (1)	
	0.016	0.011	-	0.002	-	-		0.486	

Table 2. Parameters of laser welding by solid state fiber laser YLS-5000.

Material	Sheet Thickness [mm]	Laser Power [W]	Focal Point [mm]	Welding Speed [mm·s^{-1}]	Width of FZ [1] [mm]	Width of HAZ [2] [mm]	Note
HC340LA	0.78	1700	10	50	0.9	0.35	Optimal
		2100		70	0.92	0.36	-
		2300		70	0.96	0.38	-
HCT600X	0.77	2000	10	50	2.15	0.45	Optimal
		2700		70	2.21	0.47	-
RAK40/70	0.77	2000	10	50	1.05	0.40	Optimal
		2700		70	1.17	0.48	-

[1] FZ—fusion zone, [2] HAZ—heat affected zone.

The second stage of the experimental research was focused to analyze microstructure hardness in the base metal (BM), heat affected zone (HAZ) and fusion zone (FZ). The hardness measurement was done by the Vickers method according to STN EN ISO 6507-1 on the device Duramin A300 (Struers GmbH, Willich, Germany).

The mechanical properties—yield strength, ultimate tensile strength and extension—were measured on specimens from base material and specimens with longitudinal laser weld (Figure 2) using optimized parameters of laser welding. The tests were done according to STN EN ISO 6892-1, the normal anisotropy ratio r was measured according to STN EN ISO 10113 and strain-hardening exponent n was measured according to STN EN 10275.

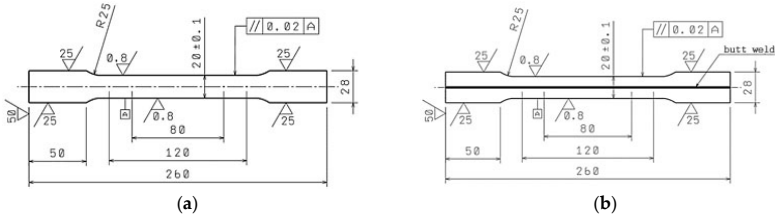

Figure 2. Specimens for tensile test: (**a**) base material; (**b**) laser-welded specimen (unit: mm).

3. Results and Discussion

3.1. Analysis of Microstructure

The microstructure of laser-welded materials in the base metal, heat affected zone and fusion zone have been analyzed for HC340LA-HC340LA, HCT600X-HCT600X and RAK40/70-RAK40/70 samples.

An overall photo of the microstructure of laser-welded steel HC340LA-HC340LA is seen in Figure 3. The overall width of the weld is approx. 1.6 mm, width of the fusion zone approx. 0.9 mm and width of the heat affected zone is approx. 0.35 mm.

The microstructure of base metal HC340LA (Figure 4) is uniform, polyhedral and fine-grained. It is composed of fine equiaxed ferrite grains, little pearlite units and tertiary cementite.

In the heat affected zone, a mostly acicular microstructure of the fusion zone comes to the polyhedral microstructure. It is created by a mixture of very fine grains of transformed ferrite, possibly bainite. Towards the base metal, in the heat affected zone, original equiaxed thicker ferrite grains are detected and their proportion is increasing (Figure 5).

A microstructure of the fusion zone is composed of ferrite, bainite and martensite in the shape of grains and needles of various sizes and shapes (Figure 6).

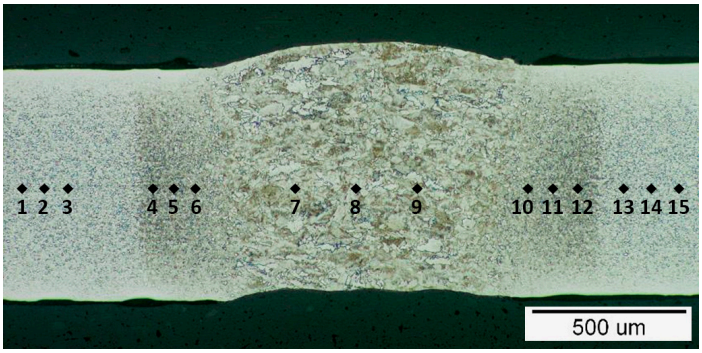

Figure 3. An overall photo of laser-welded steel HC340LA-HC340LA.

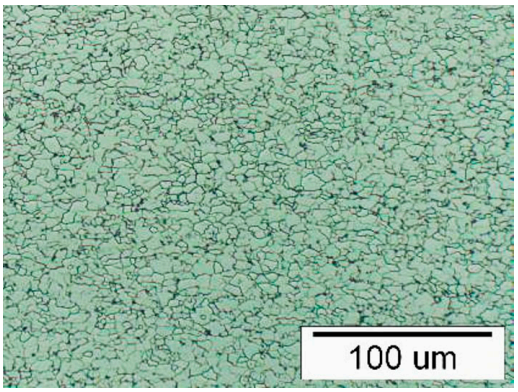

Figure 4. Microstructure of the base metal of laser-welded steel HC340LA-HC340LA.

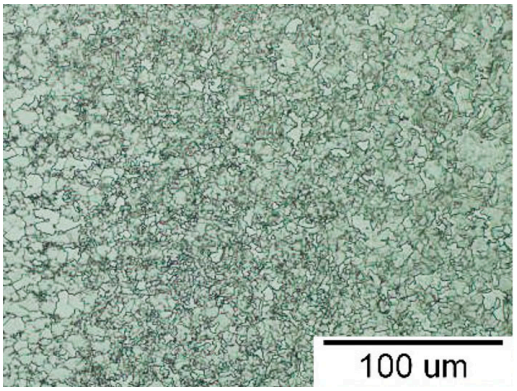

Figure 5. Microstructure of the heat affected zone of laser-welded steel HC340LA-HC340LA.

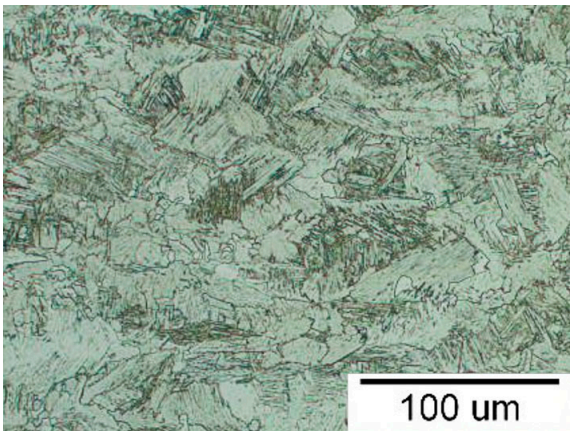

Figure 6. Microstructure of the fusion zone of laser-welded steel HC340LA-HC340LA.

An overall photo of the microstructure of laser-welded steel HCT600X-HCT600X is seen in Figure 7. The overall width of the weld is approx. 2.15 mm, width of the fusion zone is approx. 1.25 mm and width of the heat affected zone is approx. 0.45 mm.

Microstructure of base metal HCT600X is a fine-grained polyhedral made of equiaxic ferrite grains and very fine martensite grains (Figure 8). However, there are visible lines in the distribution of phases in structure and impurity particles. Tertiary cementite also occurs in the structure. The volume fraction of the martensite was 18.2 $\pm$ 2% determined by lattice method using image analyzer Image J (open source software) at a scale of 1000$\times$.

Subtilisation of martensite is visible in the heat affected zone (Figure 9). In subtle martensite, which exists in the heat affected zone, there are subtle ferrite grains, a proportion of which is increasing towards the primary material. In proximity to the primary material, the portion of ferrite grains is higher than the portion of martensite.

Due to morphology of the fusion zone microstructure, a bilateral orientation of its solidification from primary material to the welding midline is clearly seen. Microstructure of the fusion zone is composed of martensite, which was created in extended austenitic grains (Figure 10). Towards the heat affected zone, orientation of martensite laths decreases, which is a result of the decrease of a size and reduction of orientation of austenite grains, where martensite was being created.

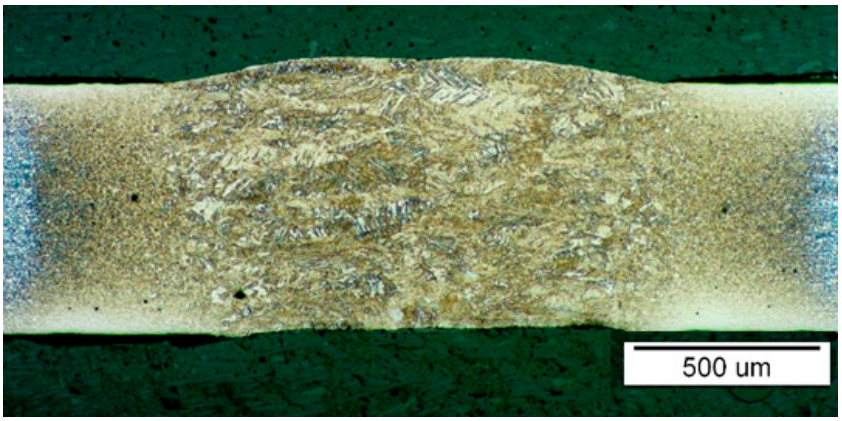

Figure 7. Overall photo of laser-welded steel HCT600X-HCT600X.

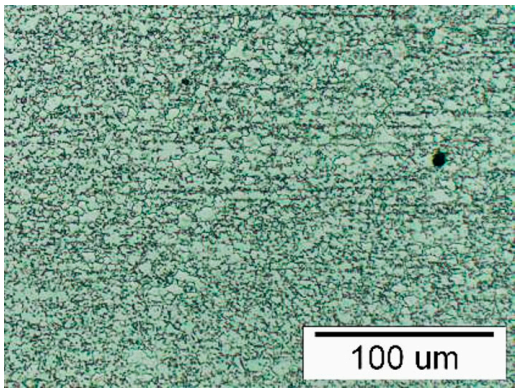

Figure 8. Microstructure of the base metal of laser-welded steel HCT600X-HCT600X.

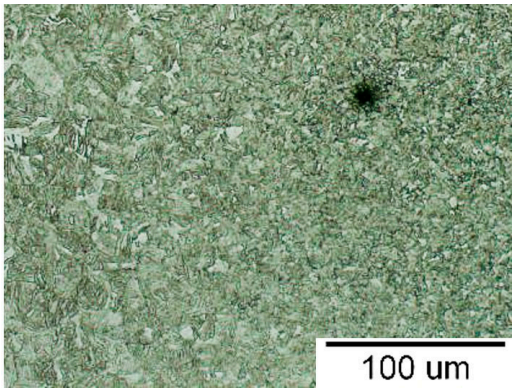

Figure 9. Microstructure of the heat affected zone of laser-welded steel HCT600X-HCT600X.

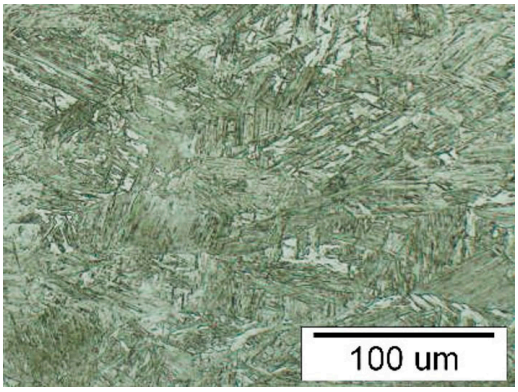

Figure 10. Microstructure of the fusion zone of laser-welded steel HCT600X-HCT600X.

An overall photo of the microstructure of laser-welded steel RAK40/70 is in Figure 11. Overall weld width is approx. 1.85 mm, width of fusion zone area is approx. 1.05 mm and width of heat affected zone is approx. 0.4 mm.

Microstructure of the base metal (Figure 12) is fine-grained, homogeneous with signs of line organization of the structure elements. It is mainly composed of fine ferrite grains and has a minority of very fine units of residual austenite, bainite and martensite. The volume fraction of residual austenite measured by RTG analysis was 22.3%. The fraction of ferrite, bainite and martensite is 77.7%. Phase components of bainite and martensite were impossible to identify due to a small distortion of lattice.

In the heat affected zone of the weld joints (Figure 13), a mixed martensite-ferrite structure occurs. The proportion of ferrite grains in this mixed microstructure increases with the distance towards primary material. In the close proximity to the primary material, in the microstructure of heat affected zone, ferrite preponderates in the form of polyhedral grains. Martensite, in the form of fine units of different shapes is in this area a minority phase.

Results of microstructural changes received when similar materials were welded comply with [5–7,20]: the fusion zone of dual phase steel consisted of fully martensitic structure; the fusion zone of high strength low alloyed steel consisted of ferrite, bainite and martensite; and the fusion zone of multi-phase steel consisted of martensite with laths oriented randomly.

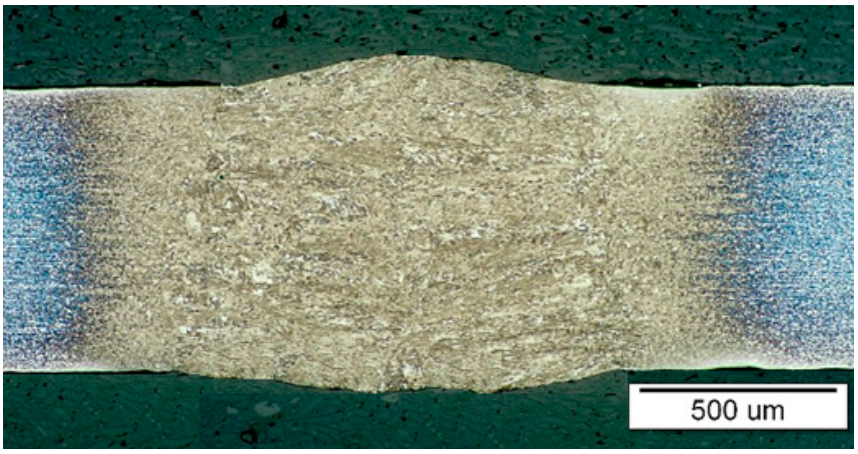

Figure 11. Overall photo of laser-welded steel RAK40/70-RAK40/70.

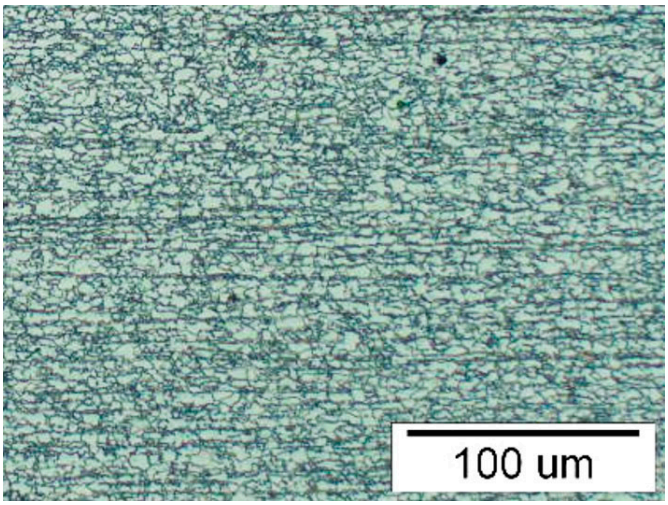

Figure 12. Microstructure of the base metal of laser-welded steel RAK40/70-RAK40/70.

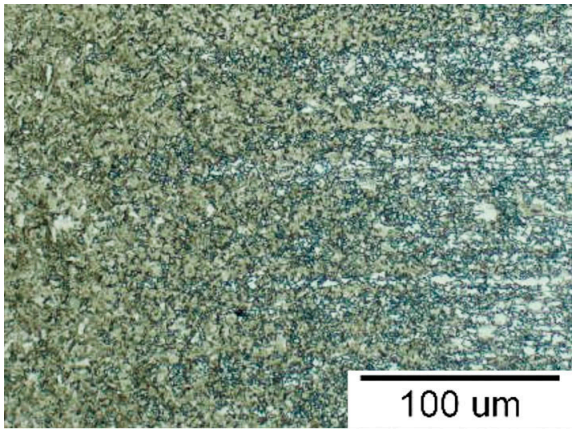

Figure 13. Microstructure of the heat affected zone of laser-welded steel RAK40/70-RAK40/70.

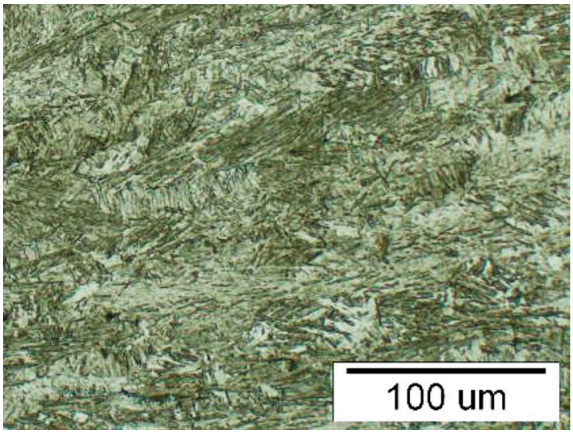

Figure 14. Microstructure of the fusion zone of laser-welded steel RAK40/70-RAK40/70.

3.2. Analysis of Microhardness and Its Distribution

The microstructure hardness was measured in the base metal (BM), heat affected zone (HAZ) and fusion zone (FZ). The hardness measurement was done by the Vickers method according to STN EN ISO 6507-1 on the device Duramin A300. The device was calibrated before measurement of microhardness HV05 on samples prepared for microstructure observation. Microhardness with load 0.5 within 10 s was automatically evaluated by software Ecos. In addition, 15 points in a row were measured on samples through the weld joint—from left to right (three points for each zone): the base metal, heat affected zone, weld joint, and heat affected zone to the base metal. The average values of HV05 microhardness and standard deviation (Stdev) for each material are shown in Table 3. The microhardness distributions in base metal, heat affected zone and fusion zone are shown in Figure 15.

Table 3. Measured values of microhardness HV05.

Material	Base Metal	Heat Affected Zone		Fusion Zone	
	HV05	HV05	HV_{HAZ}/HV_{BM}	HV05	HV_{FZ}/HV_{BM}
HC340LA	152 ± 2	183 ± 7	1.2	213 ± 3	1.4
HCT600X	205 ± 3	314 ± 49	1.5	390 ± 3	1.9
RAK40/70	219 ± 3	314 ± 56	1.4	474 ± 3	2.2

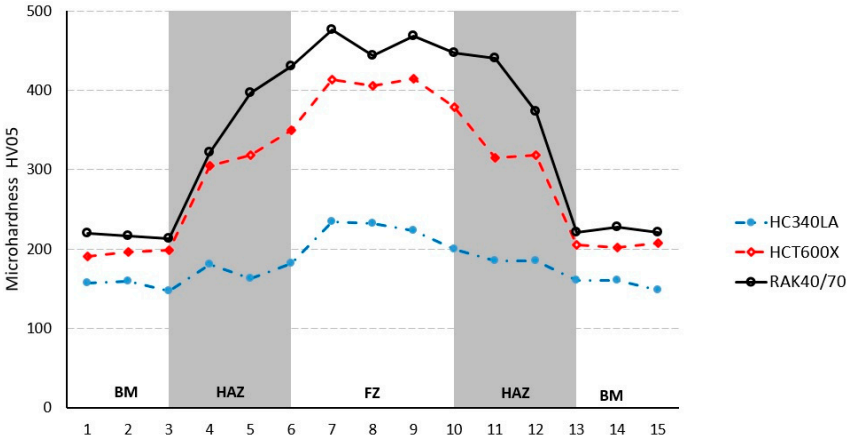

Figure 15. Microhardness distribution in the laser-welded joint.

The microhardness HV05 of base metal for HC340LA was 152 ± 2, for HCT600X, it was 205 ± 3, and for RAK40/70, it was 219 ± 3. In the transition zone between the base metal and heat affected zone, microhardness has not declined markedly, i.e., any substantial soft zone hasn't been found for each material. Otherwise, other researchers identified soft zones when thicker materials with high power were welded [5–7,20].

The microhardness HV05 of the heat affected zone laid for HC340LA-HC340LA within the interval 183 ± 7, for HCT600X-HCT600X, it was within interval 314 ± 49, and for RAK40/70-RAK40/70, it was within interval 314 ± 56. Thus, the microhardness HV05 of the heat affected zone increased for high strength low alloyed steel HC340LA 1.2 times, for dual phase steel HCT600X 1.5 times and for multi-phase steel RAK40/70 1.4 times when compared to the microhardness of base metal. Higher values of microstructure were identified for dual phase and multi-phase steels in the direction towards the fusion zone.

The highest values of microhardness for each material were measured in the fusion zone—it was for HC340LA-HC340LA within interval 213 ± 3, for HCT600X-HCT600X, it was within interval 390 ± 3, and, for RAK40/70-RAK40/70, it was within interval 474 ± 3. Hence, the microhardness HV05 of fusion zone increased for high strength low alloyed steel HC340LA 1.4 times, for dual phase steel HCT600X 1.9 times, and for multi-phase steel RAK40/70 2.2 times, when compared to the microhardness of base metal. The microhardness HV05 measured in the fusion zone for HCT600X-HCT600X and RAK40/70-RAK40/70 differ markedly, and even the welding parameters for these steels were the same. It is given by different chemical composition, i.e., carbon equivalent when calculated according to Yurioki [21,22] from chemical composition shown in Table 1—$CE_{Y\ H220PD}$ = 0.122; $CE_{Y\ HCT600X}$ = 0.397; $CE_{Y\ TRIP40/70}$ = 0.486:

$$CE_Y = C + 0.75 + 0.25\text{tangh}[20(C - 0.12)]\left[\frac{Si}{24} + \frac{Mn}{6} + \frac{Cu}{15} + \frac{Ni}{20} + \frac{Cr + Mo + Nb + V}{5}\right], \quad (1)$$

The microhardness HV05 measured in the fusion zone is well correlated to the calculated carbon equivalent CE_Y, as is shown in Figure 16.

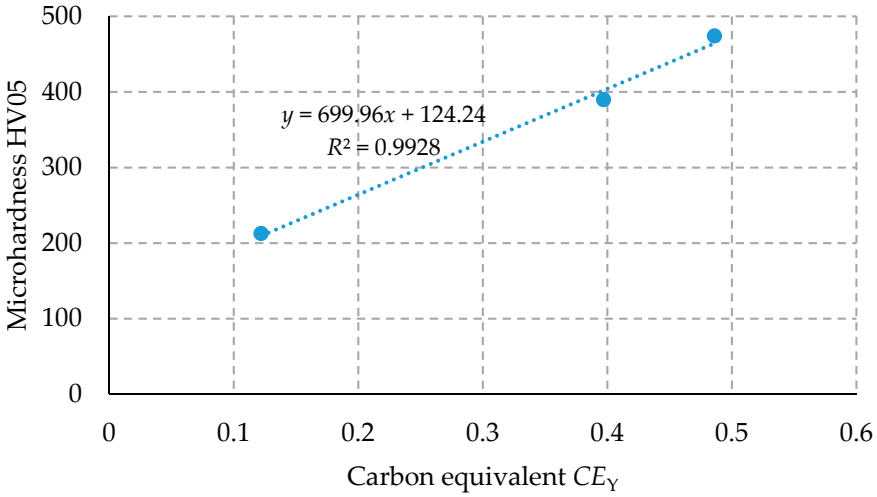

Figure 16. Microhardness distribution in the laser-welded joint.

3.3. Analysis of Mechanical Properties

Nowadays, the modern design of stampings' production is realized by numerical simulation, due to time shortening and optimization of the production process. Thus, material deformation properties have to be defined as equations describing the stress–strain relationship and material anisotropy. When simulating cold forming processes, Hill 48 yield criteria and models of stress–strain are commonly used as follows [17,23,24]:

Hill 48:

$$\sigma_{11}^2 + \sigma_{22}^2 - \frac{2 \cdot r}{1 + r}\sigma_{11}\sigma_{22} + \frac{2(1 + r)}{1 + r}\sigma_{12}^2 = \sigma_Y, \quad (2)$$

Krupkowski:

$$\sigma = K(\varphi_0 + \varphi)^n, \quad (3)$$

Hollomon:

$$\sigma = K \cdot \varphi^n, \quad (4)$$

Power law:

$$\sigma = Re + \varphi^n, \quad (5)$$

where σ_{11}, σ_{22}, σ_{12} are stress tensor components, σ_Y is yield strength, r is average normal anisotropy ratio, K is material constant, φ_0 is pre-strain, φ is logarithmic strain and n is a strain-hardening exponent. These are used with basic mechanical properties—yield strength Re, ultimate tensile strength Rm, extension A, Young modulus E, Poisson's constant μ, and density ρ.

Lankford's coefficients or normal anisotropy ratio r measured at 0°, 45° and 90° describe normal anisotropy of steel sheets as a consequence of deformation texture after rolling. These were measured according to the standard mentioned previously. Measured values of mechanical properties (Re or $R_{p0.2}$, Rm, Ag, A) and deformation properties (K, n, r) for base material and a laser-welded one are shown in Tables 4–6 for each material [25–27].

According to the stress–strain curves for base and laser-welded material (Figure 17), the considerably lowest work hardening has been found for low alloyed steel HC340LA with ferritic structure of base material (WH_{BM} 148 MPa, WH_{LW} 148 MPa), when compared to dual phase steel HTC600X with ferritic-martensitic structure of base material (WH_{BM} 374 MPa, WH_{LW} 360 MPa) or multi-phase steel RAK40/70 with ferritic-martensitic-bainitic structure of base material with residual austenite (WH_{BM} 532 MPa, WH_{LW} 483 MPa). The highest deformation hardening has been found for multi-phase steel due to phase transformation of austenite to martensite when plastically deformed. A similar tendency has been found for laser-welded samples. Comparing stress-strain curves for

laser-welded samples HC340LA-HC340LA, HTC600X-HTC600X and RAK40/70-RAK40/70, these were similar to the stress–strain curves of base material. The fracture occurred in the base material for laser-welded samples, which imply good quality of laser-welded joints.

Table 4. Mechanical properties of low alloyed steel HC340LA.

Material	Dir.	*Re* ($R_{p0.2}$) [MPa]	*Rm* [MPa]	*Ag* [%]	*A* [%]	*K*	*n*	*r*
HC340LA *	0°	378	449	17.4	28.5	728	0.178	0.66
	45°	383	455	16.8	30.4	722	0.161	0.85
	90°	389	446	18.1	29.5	724	0.169	0.76
Average		383	450	17.4	29.5	725	0.169	0.78
Stdev		5.5	4.6	0.7	1	3	0.009	0.09
HC340LA **	0°	375	447	17	29	726	0.175	0.65
	45°	380	451	16.4	30.4	718	0.157	0.84
	90°	386	440	17.3	26.5	717	0.163	0.71
Average		380	444	16.7	26	718	0.163	0.76
Stdev		5.5	5.6	0.5	2	5	0.009	0.09

* Base material, ** Laser welded.

Table 5. Mechanical properties of dual phase steel HC340LA.

Material	Dir.	*Re* ($R_{p0.2}$) [MPa]	*Rm* [MPa]	*Ag* [%]	*A* [%]	*K*	*n*	*r*
HCT600X *	0°	376	632	19	28.4	1096	0.217	0.77
	45°	378	626	19.5	28	1084	0.215	0.84
	90°	371	627	19.3	30.7	1095	0.220	0.81
Average		375	628	19.3	29	1092	0.217	0.81
Stdev		4	3	0.3	1	7	0.003	0.04
HCT600X **	0°	435	677	17	20	1109	0.182	0.76
	45°	430	672	17.3	22.3	1117	0.185	0.81
	90°	427	674	17.1	23.3	1112	0.187	0.78
Average		431	674	17.1	21.9	1112	0.185	0.79
Stdev		4	3	0.2	2	4	0.003	0.02

* Base material, ** Laser welded.

Table 6. Mechanical properties of multi-phase steel RAK40/70.

Material	Dir.	*Re* ($R_{p0.2}$) [MPa]	*Rm* [MPa]	*Ag* [%]	*A* [%]	*K*	*n*	*r*
RAK40/70 *	0°	440	764	25.3	30.3	1497	0.295	0.658
	45°	462	761	22.8	26.6	1452	0.275	0.689
	90°	457	766	24.3	29.4	1474	0.281	0.623
Average		453	764	24.1	28.8	1474	0.284	0.66
Stdev		5	3	0.8	1.5	13	0.004	0.03
RAK40/70 **	0°	466	657	20	21	1459	0.249	0.66
	45°	483	659	19	20.1	1436	0.235	0.63
	90°	474	662	20.3	22.3	1458	0.244	0.60
Average		474	659	19.8	21.1	1451	0.243	0.63
Stdev		9	2	1	1	13	0.007	0.03

* Base material, ** Laser welded.

Comparison of measured values for base material and laser welded are shown in Figure 18 for strength properties and in Figure 19 for deformation properties.

For laser-welded samples from HC340LA-HC340LA, 1% lower values of strength properties has been found (yield strength, ultimate tensile strength, material constant *K*) and deformation properties

(uniform extension *Ag*, total extension *A*, strain-hardening exponent *n*, normal anisotropy ratio *r*) as well as 5% lower value of r.n.1000 when compared to base material HC340LA.

For laser-welded samples from HTC600X-HTC600X, approx. 15% higher values of yield strength has been found, approx. 3% higher values of ultimate tensile strength and material constant *K* and lower values of deformation properties—uniform extension *Ag* approx. 12%, total extension *A* approx. 25%, strain-hardening n approx. 15%, normal anisotropy ratio *r* approx. 2% and 20% lower value of r.n.1000 when compared to base material HTC600X.

For laser-welded samples from RAK40/70-RAK40/70, approx. 5% higher values of yield strength has been found, approx. 14% lower values of ultimate tensile strength, approx. 2% lower values of material constant *K*, approx. 18% lower values of uniform extension Ag and approx. 27% lower values of total extension A, approx. 15% lower values of strain-hardening exponent *n*, approx. 5% lower values of normal anisotropy ratio r as well as 19% lower values of r.n.1000 when compared to base material RAK40/70.

It is supposed that the highest difference in strength and deformation properties for HTC600X-HTC600X and RAK40/70-RAK40/70 compared to low alloyed steel HC340LA-HC340LA is given by the volume of martensite, its morphology and distribution on each area of weld joints [23–25]. Similar results have been reached by other authors [5–7,18–20,28,29], although they used specimens with transverse laser weld and dissimilar materials were joined.

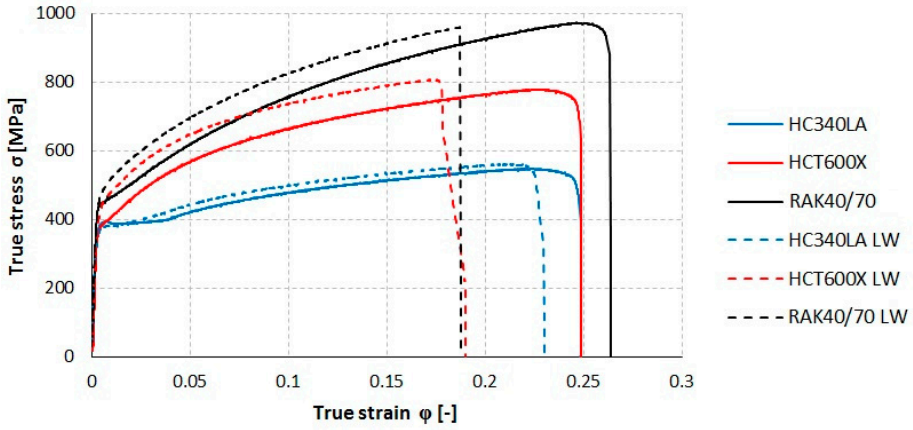

Figure 17. Stress-strain curves of base material and laser welded.

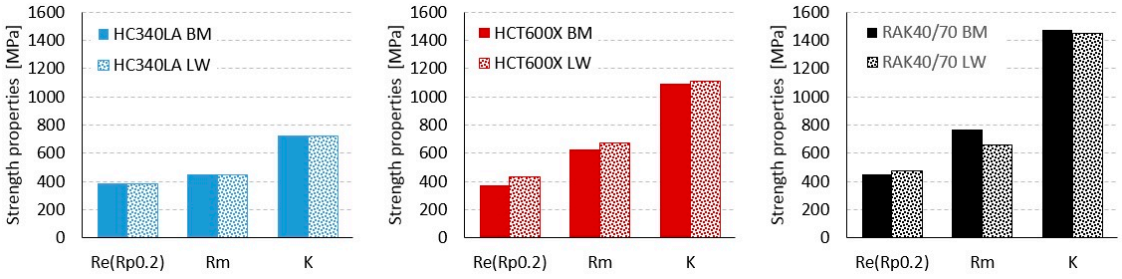

Figure 18. Strength properties of base material and laser welded.

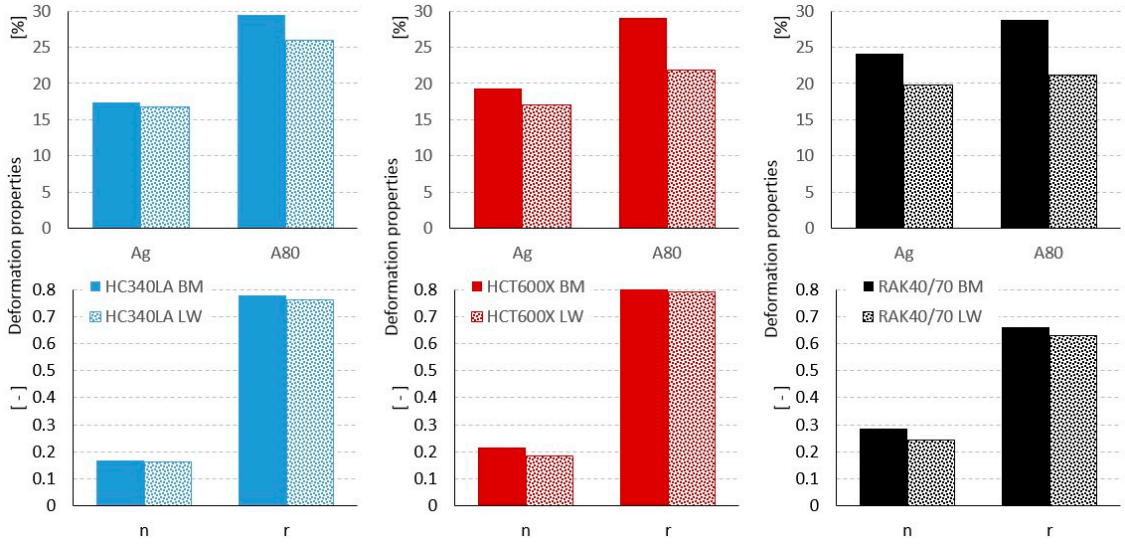

Figure 19. Deformation properties of base material and laser welded.

4. Conclusions

A wide range of metal sheets with the same or different thicknesses are joined by laser welding. However, there is a change in mechanical properties in the area of the fusion zone and the heat affected zone, due to its microstructure and width of weld joints. The experiments were focused on the research of laser welding impact on strength and deformation properties of metal sheets with thickness 0.78 mm from high strength low alloyed steel HC340LA, dual phase steel HTC600X and multi-phase steel RAK40/70, prepared as TWBs with longitudinal weld when tested.

Based on the research performed, the findings are as follows:

1. The proper quality of laser-welded joints has been reached for lower welding speed and power: 50 mm·s^{-1} and 1700 W for low alloyed steel HC340LA-HC340LA; 50 mm·s^{-1} and 2000 W for dual phase steel HTC600X-HTC600X; and 50 mm·s^{-1} and 2000 W for multi-phase steel RAK40/70-RAK40/70. This is well correlated with results presented in [18,19,28,29].
2. Laser-welded joints of experimental materials have shown proper quality of weld root and no porosity, and the good quality of joints has also been proven by tensile test, where fracture occurs in the base metal for each material.
3. Microhardness HV05 measured in samples for microstructural analysis has shown the highest values in the fusion zone for each material, and these gradually declined in heat affected zones towards the base material. Any substantial soft zone has not been found for each material. Microhardness of the fusion zone is well correlated to the carbon equivalent calculated by Yoriuki. Higher scattering of microhardness has been found for dual phase and multi-phase steel as a result of microstructure in the fusion zone and heat affected zone.
4. Stress strain curves for base material and laser-welded ones show the same tendency for each material. The highest work hardening has been found for multi-phase steel RAK40/70 due to phase transformation of austenite to martensite when plastically deformed.
5. Deformation properties are more sensitive than strength properties to the change of microstructure in the fusion zone. A greater change of uniform extension Ag and total extension A as well as a lower change of normal anisotropy ratio r and strain hardening exponent n—has been found for dual phase steel HTC600X-HTC600X and multi-phase steel RAK40/70-RAK40/70 when compared to low alloyed steel HC340LA-HC340LA. This is related to martensitic structure, its morphology and distribution in the fusion zone for dual and multi-phase steels, and ferrite, bainite (or martensite) structure in the fusion zone for high strength low-alloyed steel.

A possible solution to improve deformation properties of DP-DP, TRIP-TRIP or DP-TRIP steels can be found in their heat treatment or welding by two laser beams to reduce the cooling rate after laser welding.

Acknowledgments: The authors are grateful for the support of experimental works to Slovak Research and Development Agency, under project APVV-0273-12 "Supporting innovations of autobody components from the steel sheet blanks oriented to the safety, the ecology and the car weight reduction", as well as the grant agency for the support of the project VEGA 2/0113/16 "Influence of laser welding parameters on structure and properties of welded joints of advanced steels for the automotive industry".

Author Contributions: Emil Evin conceived and designed the experiments; Miroslav Tomáš performed the experiments of tensile tests; Emil Evin performed the experiments of microhardness tests; and Emil Evin and Miroslav Tomáš analyzed the data.

Conflicts of Interest: The authors declare no conflict of interest.

References

1. Drewes, E.J.; Prange, W. Innovative Halbzeuge für den Leichtbau mit Stahl. In *16th Steel Colloquium Aachen, "Umformtechnik, Stahl und NE-Werkstoffe-Innovative Halbzeuge—Basis für Hochleistungsprodukte"*; Verlag Mainz: Aachen, Germany, 2001; pp. 207–221.
2. Evin, E.; Tkáčová, J.; Tkáč, J. Aspects of steel sheets selection for car body components. *AI Mag. No. 2* **2012**, *5*, 88–91.
3. Evin, E.; Tkáčová, J.; Tkáč, J. Aspects of steel sheets selection for car body components. *AI Mag. No. 3* **2012**, *5*, 96–98.
4. Kvačkaj, T. Development of steels for automotive industry. In *MAT/TECH for Automotive Industry*; Technical University of Košice: Košice, Slovakia, 2015; pp. 58–67.
5. Yuce, C.; Tutar, M.; Karpat, F.; Yavuz, N. The optimization of process parameters and microstructural characterization of fiber laser welded dissimilar HSLA and MART steel joints. *Metals* **2016**, *6*, 245. [CrossRef]
6. Farabi, N.; Chen, D.L.; Zhou, Y. Microstructure and mechanical properties of laser welded dissimilar DP600/DP980 dual-phase steel joints. *J. Alloys Compd.* **2011**, *509*, 982–989. [CrossRef]
7. Mujica, L.; Weber, S.; Pinto, H.; Thomy, C.; Vollertsen, F. Microstructure and mechanical properties of laser-welded joints of TWIP and TRIP steels. *Mater. Sci. Eng. A* **2010**, *527*, 2071–2078. [CrossRef]
8. Chena, W.; Linb, G.S.; Hub, S.J. Comparison study on the effectiveness of stepped binder and weld line clamping pins on formability improvement for tailor-welded blanks. *J. Mater. Process. Technol.* **2008**, *207*, 204–210. [CrossRef]
9. Meyer, A.; Wietbrock, B.; Hirt, G. Increasing of the drawing depth using tailor rolled blanks—numerical and experimental analysis. *Int. J. Mach. Tools Manuf.* **2008**, *48*, 522–531. [CrossRef]
10. Chan, S.M.; Chan, L.C.; Lee, T.C. Tailored welded blanks of different thickness ratios effects on forming limiting diagrams. *J. Mater. Process. Technol.* **2003**, *132*, 95–101. [CrossRef]
11. Merklein, M.; Lechner, M. Manufacturing flexibilisation of metal forming components by tailored blanks. In Proceedings of the COMA 13th International Conference on Competitive Manufacturing, Stellenbosch, South Africa, 30 January–1 February 2013; pp. 1–6.
12. Monaco, A.; Sinke, J.; Benedictus, R. Experimental and numerical analysis of a beam made of adhesively bonded tailor-made blanks. *Int. J. Adv. Manuf. Technol.* **2009**, *44*, 766–780. [CrossRef]
13. Reisgen, U.; Schleser, M.; Mokrov, O.; Ahmed, E. Statistical modeling of laser welding of DP/TRIP steel sheets. *Opt. Laser Technol.* **2012**, *44*, 92–101. [CrossRef]
14. Sennaroglu, A. *Solid-State Lasers and Applications*, 1st ed.; CRC Press: Boca Raton, FL, USA, 2007.
15. Koechner, W.; Bass, M. *Solid-State Lasers: A Graduate Text*, 1st ed.; Springer: New York, NY, USA, 2003.
16. Hyrcza-Michalska, M.; Grosman, F. The evaluate of laser welded tailor and tubular blanks formability for automotive vehicle elements stamping. *Arch. Civ. Mech. Eng.* **2009**, *9*, 69–81. [CrossRef]
17. Piela, A.; Lisok, J.; Rojek, J. Experimental study and numerical simulation of tailor welded blanks. In Proceedings of the International Conference on Advanced Materials & Processing Technologies AMPT 2003, Dublin, Ireland, 8–11 July 2003.
18. Esquivel, A.S.; Nayak, S.S.; Xia, M.S.; Zhou, Y. Microstructure, hardness and tensile properties of fusion zone in laser welding of advanced high strength steels. *Can. Metall. Q.* **2012**, *51*, 328–335. [CrossRef]

19. Švec, P.; Schrek, A.; Hrnčiar, V.; Csicsó, T. Fibre laser welding of dual phase steels. *Acta. Metall. Slovaca* **2015**, *21*, 311–320. [CrossRef]
20. Saha, D.C.; Westerbaan, D.; Nayak, S.S.; Biro, E.; Gerlich, A.P.; Zhou, Y. Microstructure-properties correlation in fiber laser welding of dual-phase and HSLA steels. *Mater. Sci. Eng. A* **2014**, *607*, 445–453. [CrossRef]
21. Yurioka, N.; Okumura, M.; Kasuya, T.; Cotton, H. Prediction of HAZ hardness of transformable steels. *Met. Constr.* **1987**, *4*, 217R–223R.
22. Yurioka, N.; Kasuya, T. A chart method to determine necessary preheat temperature in steel welding. *Q. J. Jpn. Weld. Soc.* **1995**, *13*, 347–357.
23. ESI Group. *PAM-STAMP 2G 2011: Users's Guide*, 1st ed.; ESI Group: Paris, France, 2010.
24. Banabic, D. *Sheet Metal Forming Processes: Constitutive Modelling and Numerical Simulation*, 1st ed.; Springer: Berlin, Germany, 2010.
25. Evin, E.; Tomáš, M. *Annual Report of the Project APVV-0273-12*; Technical University of Kosice: Kosice, Slovakia, 2014.
26. Evin, E.; Tomáš, M. *Annual Report of the Project APVV-0273-12*; Technical University of Kosice: Kosice, Slovakia, 2015.
27. Evin, E.; Tomáš, M. *Annual Report of the Project APVV-0273-12*; Technical University of Kosice: Kosice, Slovakia, 2016.
28. Zhang, C.H.; Song, X.; Lu, P.; Hu, X. Effect of microstructure on mechanical properties in weld-repaired high strength low alloy steel. *Mater. Des.* **2012**, *36*, 233–242. [CrossRef]
29. Singh, S.; Nanda, T.; Ravi Kumar, B.; Singh, V. Controlled phase transformation simulations to design microstructure for tailored mechanical properties in steel. *Mater. Manuf. Process.* **2016**, *31*, 2064–2075. [CrossRef]